Accelerated evolution of convective simulations

Evan H. Anders and Benjamin P. Brown
Dept. Astrophysical & Planetary Sciences, University of Colorado – Boulder, Boulder, CO 80309, USA and Laboratory for Atmospheric and Space Physics, Boulder, CO 80303, USA

Jeffrey S. Oishi
Department of Physics and Astronomy, Bates College, Lewiston, ME 04240, USA

We present a method for coupling boundary value problems with initial value problems in order to achieve Accelerated Evolution (AE) of convective solutions on dynamical timescales, rather than the long thermal timescale. We study this method in the context of Rayleigh-Bénard convection. We demonstrate that the solution reached by AE and Standard Evolution (SE) are similar, and that this method works at a large range of supercriticalities. The AE method is used to achieve converged solutions at high supercriticality (10^7), and its extensions to more complex systems are briefly discussed.

I. INTRODUCTION

Natural convection occurs in the presence of disparate timescales which prohibit numericists from studying realistic models of natural systems. For example, flows in the convection zones of stars like the Sun are characteristically low Mach number (Ma) in the deep interior. Explicit timestepping methods which are bound by the Courant-Friedrich-Lewy (CFL) timestep limit must resolve the fastest motions (sound waves), resulting in timesteps which are prohibitively small for studies of the deep, low-Ma motions. These systems are numerically stiff, and the difference between the sound crossing time and the convective overturn time have made studies of low-Ma stellar convection difficult. Traditionally, approximations such as the anelastic approximation, in which sound waves are explicitly filtered out, have been used to study low-Ma flows [1, 2]. More recently, advanced numerical techniques which use implicit or mixed implicit-explicit timestepping mechanisms have made it feasible to study convection at low Mach numbers [3–8], and careful studies of deep convection which would have been impossible a decade ago are now widely accessible.

Convective systems with divergent dynamical timescales can now be studied; however, thermal timescales, which characterize system relaxation, are often much larger than dynamical timescales, and resolving dynamics in atmospheres which are sufficiently thermally relaxed remains a challenging problem. Solar convection is a prime example of this phenomenon. Dynamical timescales in the solar convective zone are relatively short (10 min overturn at solar surface, one month solar rotation rate) compared to the Sun's Kelvin-Helmholtz timescale of $3 \cdot 10^7$ years [9]. In such a system, it is impossible to resolve the convective dynamics while also evolving the thermal structure of the system in a meaningful fashion using traditional timestepping techniques alone. As modern simulations aim to model natural convection by increasing into the high-Rayleigh-number (Ra) regime, the thermal diffusion timescale becomes intractably large compared to dynamical timescales [7]. Furthermore, as dynamical and thermal timescales separate, simulations become more turbulent. Increasingly turbulent motions require finer grid meshes and smaller timesteps to capture advective dynamics. Thus, the progression of simulations into the high-Ra regime of natural convection is slowed by two simultaneous effects: timestepping through a single convective overturn time becomes more computationally expensive and the number of overturn times required for systems to reach thermal equilibration grows.

The vast difference between convective and thermal timescales has long plagued numericists studying convection, and an abundance of approaches has been employed to study thermally converged solutions. One popular method for accelerating the convergence of high-Ra solutions is by "bootstrapping" – the process of using the flow fields in a converged solution at low Ra as initial conditions for a simulation at high Ra. This method has been used with great success [10, 11], but it is not without its faults. Bootstrapped solutions are succeptible to hysteresis effects, in which large-scale convective structures present in the low Ra solution imprint onto the dynamics of the new, high Ra solution. Another commonly-used tactic in moderate-Ra simulations is to use a simple model of the full convective state as initial conditions. For example, past studies have used a linear eigenvalue solve to set the initial convective state [12] or used an axisymmetric solution as initial conditions for convection in a 3D cylinder [11]. In other systems, the approximate state of the evolved solution can be estimated. There, a set of initial conditions which is close to the evolved state be derived analytically [13, 14].

Despite the numerous methods that have been used, the most straightforward way to achieve a thermally converged solution is to evolve a convective simulation through a thermal timescale. Some modern studies do just that [2]. However, such evolution is *expensive*, and state-of-the-art simulations at the highest values of Ra can only reasonably

be run for tens to hundreds of buoyancy times [15], much less the thousands of buoyancy timescales required for thermal convergence.

In this work, we study a method of achieving accelerated evolution of convective simulations. We couple measurements of the dynamics of non-converged convective simulations with knowledge about energy balances in the desired solution to self-consistently adjust the mean thermodynamic profile towards its evolved state. While such a method has been used previously [16], we find no explanation in the current literature of the steps involved in employing this method, nor any study into the accuracy of such a method. In section II, we describe our convective simulations, our numerical methods, and our method for achieving accelerated evolution. In section III, we compare solutions reached through the accelerated evolution method to those that have been evolved through a full diffusive timescale, and we examine select simulations at high Ra which have achieved accelerated evolution. Finally, in section IV, we discuss extensions of the methods presented here, and we offer concluding remarks.

II. EXPERIMENT

We study incompressible Rayleigh-Bénard convection under the Oberbeck-Boussinesq approximation, such that our fluid has a constant kinematic viscosity (ν), thermal diffusivity (κ), and coefficient of thermal expansion (α). The density of the fluid is a constant, ρ_0, except where it is $\rho = \rho_0(1-\alpha T_1)$ on the term where the constant gravitational acceleration, $\boldsymbol{g} = -g\hat{z}$, acts in the vertical momentum equation. The equations of motion are [17]

$$\nabla \cdot \boldsymbol{u} = 0, \tag{1}$$

$$\frac{\partial \boldsymbol{u}}{\partial t} + \boldsymbol{u}\cdot\nabla\boldsymbol{u} = -\frac{1}{\rho_0}\nabla P - g(1-\alpha T_1)\hat{z} + \nu\nabla^2\boldsymbol{u}, \tag{2}$$

$$\frac{\partial T_1}{\partial t} + \boldsymbol{u}\cdot\nabla(T_0+T_1) = \kappa\nabla^2 T_1, \tag{3}$$

where $\boldsymbol{u} = u\hat{x} + v\hat{y} + w\hat{z}$ is the velocity, $T = T_0 + T_1$ are the initial and fluctuating components of temperature, and P is the pressure. We non-dimensionalize these equations such that the length is in units of the layer height (L_z), temperature is in units of the initial temperature jump across the layer ($\Delta T_0 = L_z\nabla T_0$), and velocity is in units of the freefall velocity ($v_{\rm ff} = \sqrt{\alpha g L_z^2 \nabla T_0}$). by these choices, one time unit is a freefall time ($L_z/v_{\rm ff}$). We introduce a reduced kinematic pressure, $\varpi \equiv (P/\rho_0 + \phi + |\boldsymbol{u}|^2/2)/v_{\rm ff}^2$, where the gravitational potential, ϕ, is defined such that $\boldsymbol{g} = -\nabla\phi$. As P is a Langrange multiplier under the Oberbeck-Boussinesq approximation, ϖ can be treated straightforwardly as a linear variable. In non-dimensional form, Eqns. 2 & 3 become

$$\frac{\partial \boldsymbol{u}}{\partial t} + \nabla\varpi - T_1\hat{z} + \mathcal{R}\nabla\times\boldsymbol{\omega} = \boldsymbol{u}\times\boldsymbol{\omega}, \tag{4}$$

$$\frac{\partial T_1}{\partial t} - \mathcal{P}\nabla^2 T_1 + w\frac{\partial T_0}{\partial z} = -\boldsymbol{u}\cdot\nabla T_1, \tag{5}$$

where $\boldsymbol{\omega} = \nabla\times\boldsymbol{u}$ is the vorticity. The dimensionless control parameters $\mathcal{P}$ and $\mathcal{R}$ are set by the Rayleigh and Prandtl numbers,

$$\mathcal{R} \equiv \sqrt{\frac{\rm Pr}{\rm Ra}}, \qquad \mathcal{P} \equiv \frac{1}{\sqrt{\rm Pr\,Ra}}, \qquad {\rm Ra} = \frac{g\alpha L_z^4 \nabla T_0}{\nu\kappa} = \frac{(L_z\, v_{\rm ff})^2}{\nu\kappa}, \qquad {\rm Pr} = \frac{\nu}{\kappa}. \tag{6}$$

We hold Pr= 1 constant throughout this work, such that $\mathcal{P} = \mathcal{R}$.

We study 2D and 3D convection in which the domain is a cartesian box, whose dimensionless vertical extent is $z \in [-1/2, 1/2]$, and which is horizontally periodic with an extent of $x, y \in [0, \Gamma]$, where $\Gamma = 2$ is the aspect ratio. In 2D simulations, we set $v = \partial_y = 0$. We specify no-slip, impenetrable boundary conditions at both the top and bottom boundary and we use mixed thermal boundary conditions, such that

$$u = v = w = 0 \text{ at } z = \pm 1/2, \qquad T_1 = 0 \text{ at } z = +1/2, \qquad \frac{\partial T_1}{\partial z} = 0 \text{ at } z = -1/2. \tag{7}$$

For this choice of boundary conditions, the critical value of Ra at which the onset of convection occurs is ${\rm Ra_{crit}} = 1295.78$, and the supercriticality of a run is defined as $S \equiv {\rm Ra/Ra_{crit}}$. Studies of convection which aim to model astrophysical systems such as stars often employ mixed thermal boundary conditions [12, 18, 19], as we do here; however, our choice of thermal boundary conditions here reflects the fact that the conditions in Eqn. (7) are the simplest to implement in the process of accelerated evolution (see section II A) we study here.

We utilize the Dedalus[1] pseudospectral framework [20] to evolve Eqns. (1), (4), & (5) forward in time using an implicit-explicit (IMEX), third-order, four-step Runge-Kutta timestepping scheme RK443 [21]. The linear terms (on the LHS of the equations) are solved implicitly, while the nonlinear terms (RHS) are explicitly solved. Variables are time-evolved on a dealiased Chebyshev (vertical) and Fourier (horizontal, periodic) domain in which the physical grid dimensions are 3/2 the size of the coefficient grid.

As initial conditions, we fill T_1 with random white noise whose magnitude is $10^{-6}\mathcal{P}$. This ensures that the initial perturbations are much smaller than the evolved convective temperature perturbations, even at large Ra. We filter this noise spectrum in coefficient space, such that only the lower 25% of the coefficients have power.

A. The method of Accelerated Evolution

Here we describe a method of Accelerated Evolution (AE), which we use to rapidly evolve the thermodynamic state of convective simulations. We compare this AE method to Standard Evolution (SE), in which we naively evolve the atmosphere for one thermal diffusion time, $t_\kappa = \mathcal{P}^{-1}$. As Ra increases, SE solutions become intractable, while the timeframe of convergence for an AE solution remains nearly constant in freefall time units. For an example of time saving achieved by using AE, we compare energy traces at $S = 10^5$ from a SE run in Fig. 1a to an AE run in Fig. 1c.

The horizontally averaged profiles of the vertical conductive flux, $\mathrm{F}_{\mathrm{cond}} = \langle -\kappa\nabla(T_0 + T_1)\rangle_{x,y}$, and the vertical convective flux, $\mathrm{F}_{\mathrm{conv}} = \langle w(T_0 + T_1)\rangle_{x,y}$, where $\langle\rangle_{x,y}$ represent a horizontal average, are the basis of the AE method. We measure both of these quantities early in a simulation, retrieving profiles similar to those shown in Fig. 1b. At early stages in the simulation, these flux profiles are highly asymmetric, with more flux exiting the atmosphere at the upper boundary than the fixed-flux lower boundary is providing. By calculating the total flux, $\mathrm{F}_{\mathrm{tot}} = \mathrm{F}_{\mathrm{conv}} + \mathrm{F}_{\mathrm{cond}}$, we derive the profiles

$$f_{\mathrm{conv}}(z) = \frac{F_{\mathrm{conv}}}{F_{\mathrm{tot}}}, \qquad f_{\mathrm{cond}}(z) = \frac{F_{\mathrm{cond}}}{F_{\mathrm{tot}}}, \tag{8}$$

which have the systematic asymmetries removed. These profiles describe which parts of the atmosphere depend on convection to carry flux (where $f_{\mathrm{conv}}(z) = 1$ and $f_{\mathrm{cond}}(z) = 0$). We presume that the early convection occupies roughly the same volume as the evolved convection, and thus that the extent of the early thermal boundary layers (where $f_{\mathrm{cond}}(z) = 1$ and $f_{\mathrm{conv}}(z) = 0$) will not change significantly over the course of the atmosphere's evolution. Under this assumption, the proper evolved atmospheric flux profiles are $\mathrm{F}_{\mathrm{conv,\,ev}} = \mathrm{F}_{\mathrm{bot}} \cdot f_{\mathrm{conv}}$ and $\mathrm{F}_{\mathrm{cond,\,ev}} = \mathrm{F}_{\mathrm{bot}} \cdot f_{\mathrm{cond}}$, where $\mathrm{F}_{\mathrm{bot}} = \mathcal{P}$ is the amount of flux entering the bottom of the atmosphere.

In a time-stationary state, the horizontal- and time-average of Eqns. (4) and (5), neglecting terms which vanish due to symmetry, are

$$\frac{\partial}{\partial z}\langle\varpi\rangle_{x,y} - \langle T_1\rangle_{x,y}\,\hat{z} = \langle \boldsymbol{u}\times\boldsymbol{\omega}\rangle_{x,y}\,, \tag{9}$$

$$\frac{\partial}{\partial z}\mathrm{F}_{\mathrm{conv,\,ev}} - \mathcal{P}\frac{\partial^2}{\partial z^2}\langle T_1\rangle_{x,y} = 0. \tag{10}$$

Convective flows are perturbations around a thermal profile defined by these equations in the proper evolved, statistically stationary state. Furthermore, under the specification of $\mathrm{F}_{\mathrm{conv,\,ev}}$ and $\langle \boldsymbol{u}\times\boldsymbol{\omega}\rangle_{x,y}$, *the mean thermodynamic structure of the system is fully specified.*

Thus, the AE method is simple: we construct $\mathrm{F}_{\mathrm{conv,\,ev}}$ as described above. Then we calculate a profile, $\xi(z) = \mathrm{F}_{\mathrm{conv,\,ev}}/\mathrm{F}_{\mathrm{conv}}$, which is the fraction, as a function of height, by which the flux in the system must be reduced to go from an initial state (Fig. 1b) to an evolved state (Fig. 1d). We multiply the velocities and the thermal fluctuations, $T - \langle T\rangle_{x,y}$, by $\sqrt{\xi}$, such that the advected, flux-carrying perturbations in the temperature are appropriately diminished. We then solve a boundary value problem including Eqns. (9) & (10) using $\mathrm{F}_{\mathrm{conv,\,ev}}$ and $\cdot\,\langle \boldsymbol{u}\times\boldsymbol{\omega}\rangle_{x,y}$, after diminishing it by a factor of ξ. We use mixed thermal boundary conditions, as in Eqn. (7), because F_{bot} is exactly specified, and the temperature profile is pegged at a reference value for the AE solve. For specifics on the precise implementation of the AE method, we refer the reader to appendix A.

The AE method converges atmospheeres from extreme flux disequilibrium states (Fig. 1b) on short dynamical timescales (Fig. 1c) to a converged state (Fig. 1d) whose flux balance is very close to the balance present in the corresponding SE solution (Fig. 1e). While the application of the AE method advances solutions toward the proper solution, we find that multiple applications of the method is the best means of achieving converged solutions quickly.

[1] http://dedalus-project.org/

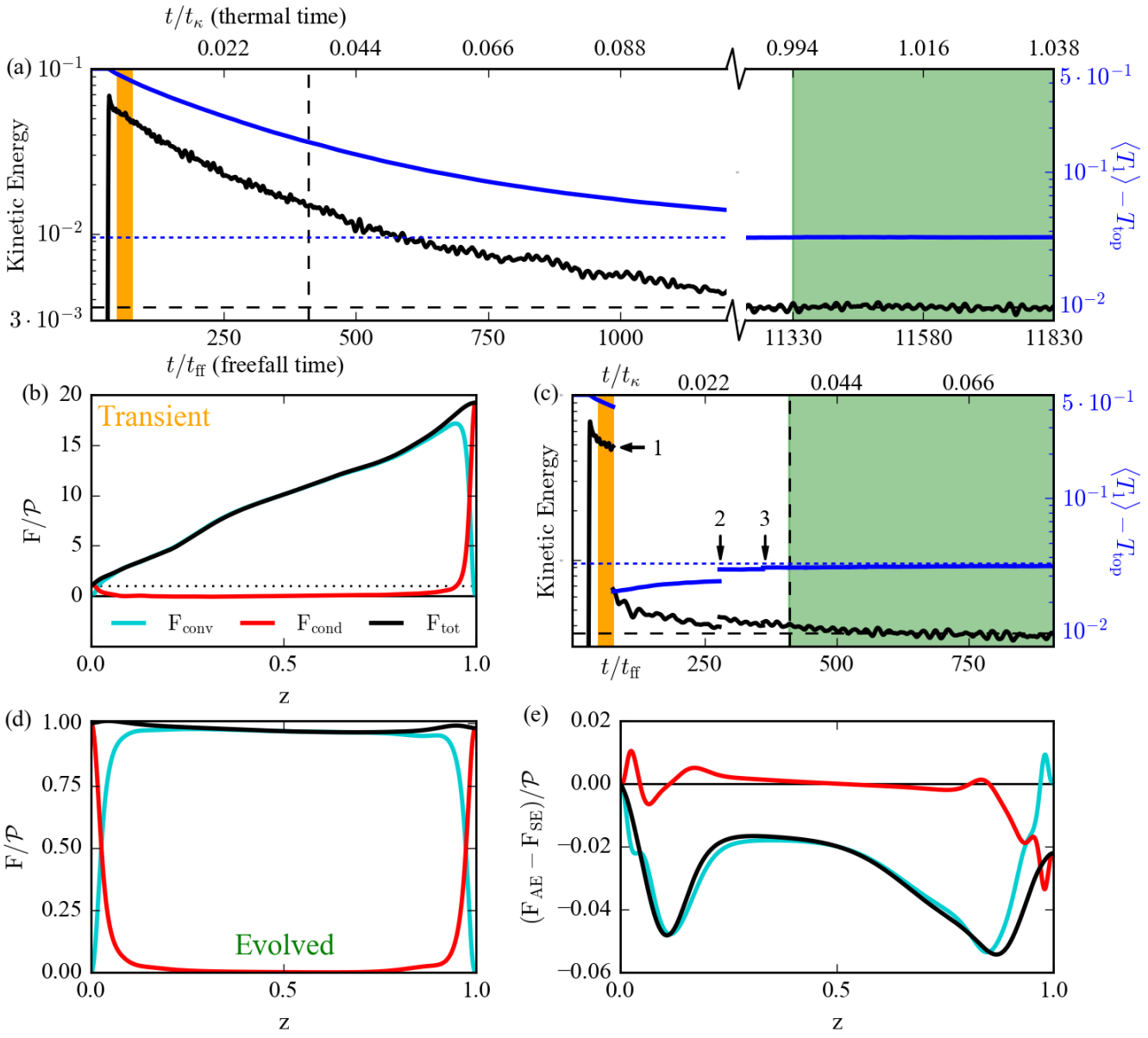

FIG. 1. A time trace is shown of kinetic energy (black) and mean temperature (blue) vs. time for an SE run at $S = 10^5$ (a). The mean evolved values of kinetic energy and mean temperature are denoted by the horizontal dashed black and blue lines. By taking an average of the fluxes early in the simulation (b), and appropriately using the AE method described here, the evolution of these atmospheres can be greatly accelerated. The time trace of such an accelerated atmosphere, which uses these methods, is shown in (c). The y-axes and x-axes are scaled identically as in (a). Here, the AE method is used three times, marked by the numbered arrows. The fluxes averaged over the green region which begins at the vertical dashed line shortly after AE 3 are shown in (c) are shown in (d), and they are nearly in the fully evolved state, sampled over a similarly long region that occurs much later in the simulation in (a). The difference between the fluxes in the AE and SE ssolutions is shown in (e), and it is small. The dashed vertical line in (a) denotes the simulation time at which evolved flux measurements begin to be taken in (c).

III. RESULTS

We study evolved solutions achieved through the standard evolution (SE) method from convective onset up to $S = 10^5$ in 2D and $S = 10^4$ in 3D. These SE runs are compared to accelerated evolution (AE) runs spanning from onset up to $S = 10^7$ in 2D and $S = 10^4$ in 3D. For a full list of simulations, we refer the reader to appendix B.

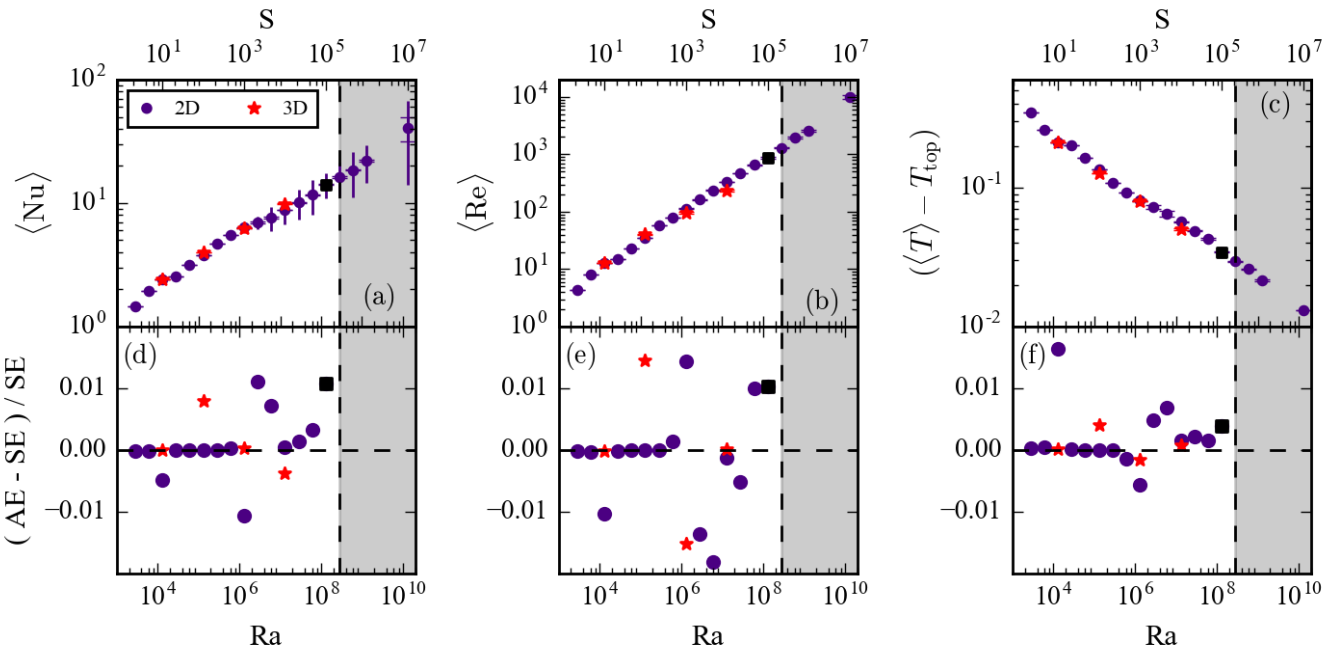

FIG. 2. Volume- and time-averaged measurements of the Nusselt number, the RMS Reynolds number, and the mean temperature for AE runs are shown in (a)-(c). Symbols are located at the mean value of each measurement, vertical lines represent the standard deviation of the measurement, which shows natural variation over the averaging window, and error bars represent the change in the mean value over the averaging window, such that very large error bars represent solutions which are not fully converged when averaging begins. (a) The Nusselt number scales as $\mathrm{Ra}^{1/5}$, and above $\mathrm{S} \geq 10^{3+2/3}$, simulations exhibit oscillating plume structures whose heat transport varies over time. (b) The RMS Reynolds number, which measures the level of turbulence in the evolved solution, scales as $\mathrm{Ra}^{0.45}$. (c) Temperature, with its value at the upper boundary removed, is shown, and scales as $\mathrm{Ra}^{-1/5}$. Relative error for (d) Nu, (e) Re, and (f) T are shown between measurements taken in AE solutions and SE solutions. The greyed area of the plot indicates the region in which only AE runs were carried out due to computational expense. The run at $S = 10^5$ marked as a black square is examined in more details in Figs. 1, 3, & 4.

We report the time- and volume-averaged values of select measurements of the evolved solutions in Fig. 2. The scaling of heat transport in the evolved solution, as quantified by the Nusselt number, is shown in Fig. 2a. The volume averaged Nusselt number is defined as

$$\mathrm{Nu} = \frac{\langle F_{\mathrm{conv}} + F_{\mathrm{cond}} \rangle}{\langle F_{\mathrm{cond,\ ref}} \rangle} = \frac{\langle wT - \mathcal{P}\partial_z T \rangle}{\langle -\mathcal{P}\partial_z T \rangle}, \tag{11}$$

where $\langle\rangle$ represent a volume average. In 2D when $S < 10^{3+2/3}$ and in 3D, the evolved system is defined by a clear value of Nu and the convective heat transport reaches a temporally stationary state. In 2D and at larger values of S, the value of Nu oscillates as a function of time due to large horizontal oscillations in the convective plume structures. Our choice of no-slip boundary conditions prevent the fluid from entering a shearing state [22], but the oscillatory motions which do arise cause the system to vary between periods of low heat transport and high heat transport. The SE simulations which span up to $S = 10^5$ exhibit the same horizontally oscillatory motion as the AE solutions for the same initial conditions. The scaling of the mean value of Nu is roughly $\mathrm{Nu} \propto \mathrm{Ra}^{1/5}$, weaker than that reported in similar systems with fixed-T and fixed-flux boundary conditions [10]. We attribute this weaker Nu scaling to the oscillatory nature of the plumes, which may have been avoided by previous studies using bootstrapping techniques as initial conditions.

In Fig. 2b, we report the volume-averaged RMS Reynolds number in the AE solutions, where $\mathrm{Re} = \langle |\boldsymbol{u}| \rangle / \mathcal{R}$. This measure scales roughly as $\mathrm{Re} \propto \mathrm{Ra}^{0.45}$, and shows little variance with time.

In Fig. 2c, we report the volume averaged temperature of the AE solutions, with the value at the upper (fixed T) boundary removed. This measurement probes the thickness of the boundary layers of the solutions, and should show scaling which is inversely proportional to Nu in converged solutions where fixed-flux boundary conditions are used [23]. We find here that $(\langle T \rangle - T_{\mathrm{top}}) \propto \mathrm{Ra}^{-1/5}$, precisely the inverse scaling of Nu, giving confidence that these solutions are in a converged state.

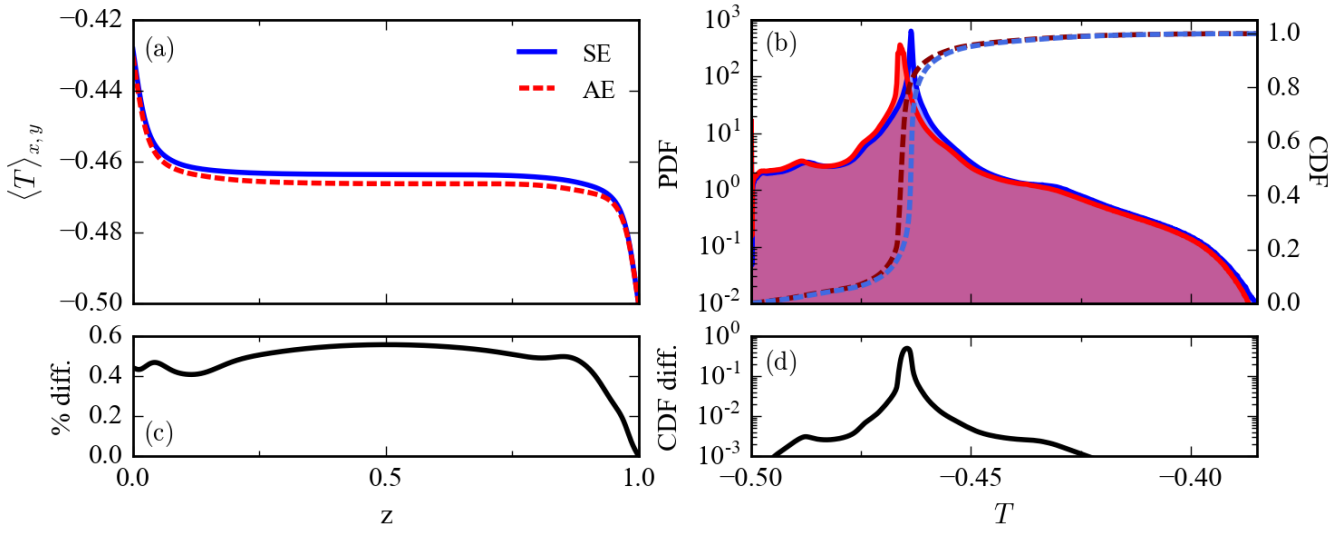

FIG. 3. Comparisons of the evolved thermodynamic states of an AE and SE run at $S = 10^5$ are shown. (a) Evolved horizontally- and time-averaged temperature profiles, as a function of height. (b) Probability Distribution Functions (PDFs) and their integrated Cumulative Distribution Functions (CDFs) of point-by-point measurements of the temperature field. (c) The percentage difference between the mean temperature profiles as a function of height. (d) The value of the Kolmogorov-Smirnov (KS) statistic, or the difference between the AE and SE CDFs, as a function of temperature. T is sampled every 0.1 time units for 500 total time units, and was interpolated onto an evenly spaced grid before sampling. The difference between the mean profiles is very small O(0.5%), but this small difference results in a large difference between the two temperature CDFs near the values of the temperature mode. The spread of temperature around the mode, or the fluctuations that drive convection, are nearly identical between the two runs.

In Fig. 2d-f, we report the fractional difference between measurements from the AE solutions and measurements from the SE solutions. We find that the mean value of Nu from AE solutions is accurate to the values from SE solutions to within $\sim 1\%$, and the same is true for $\langle T \rangle$ measurements. Re measurements show slightly greater error, with AE measurements being on average $\leq 2\%$ away from the SE measurements.

The measurements presented in Fig. 2 demonstrate that the AE method can be powerfully employed in parameter space studies in which large numbers of simulations are compared in a volume-averaged sense. We now turn our examination to a more direct comparison of AE and SE for convection at $S = 10^5$, as has been introduced in Fig. 1.

As the AE method primarily serves to adjust the thermodynamic structure of the solution, we compare the temperature profile attained by AE and SE in Fig. 3. We see that the boundary layer length scale is nearly identical between the two solutions (Fig. 3a), but that the mean temperature in the interior differs by about 0.5% on average (Fig. 3c).

The probability distribution functions of point-by-point temperature measurements are compared for the two runs in Fig. 3b. We construct this PDF from snapshots of the temperature profile every 0.1 freefall time units over a duration of 500 total freefall time units, as shown by the green areas if Fig. 1a&c. We interpolate the temperature field of each of these snapshots onto an evenly spaced grid, determine the frequency distribution of all measured T values, and then normalize the distribution such that its integral is unity. The primary difference between the two PDFs is their modes, which is expected from Fig. 3a. The fact that the the AE temperature profile is roughly 0.5% off of the SE temperature profile (3c), the AE temperature field is still marginally evolving towards the SE temperature field, and this evolution appears as asymmetry of the AE PDF's peak.

One means of comparing two probability distributions to determine if they are drawn from the same underlying sample is through the use of a Kolmogorov-Smirnov (KS) [24]. In general, a KS test must be conducted on independent, uncorrelated data, which poorly describes the point-by-point values of flow in a fluid simulation. Thus, we will merely use the KS statistic, the maximum difference between the cumulative distribution functions (CDFs) of the two sample distributions, as a numerical method of directly comparing the two PDFs. For the distributions shown in Fig. 3b, the difference between the CDFs is shown in Fig. 3d. The maximum difiference, or the KS statistic, is 0.495 near the modes. This difference is very large, but is not unexpected. While the temperature distributions near the modes are very different, their spread of perturbations is nearly identical.

In addition to comparing the thermodynamic state achieved by the SE and AE methods, we examine the velocities found in the evolved states. We compute PDFs in the same manner as in Fig. 3b for the vertical velocity (Fig.

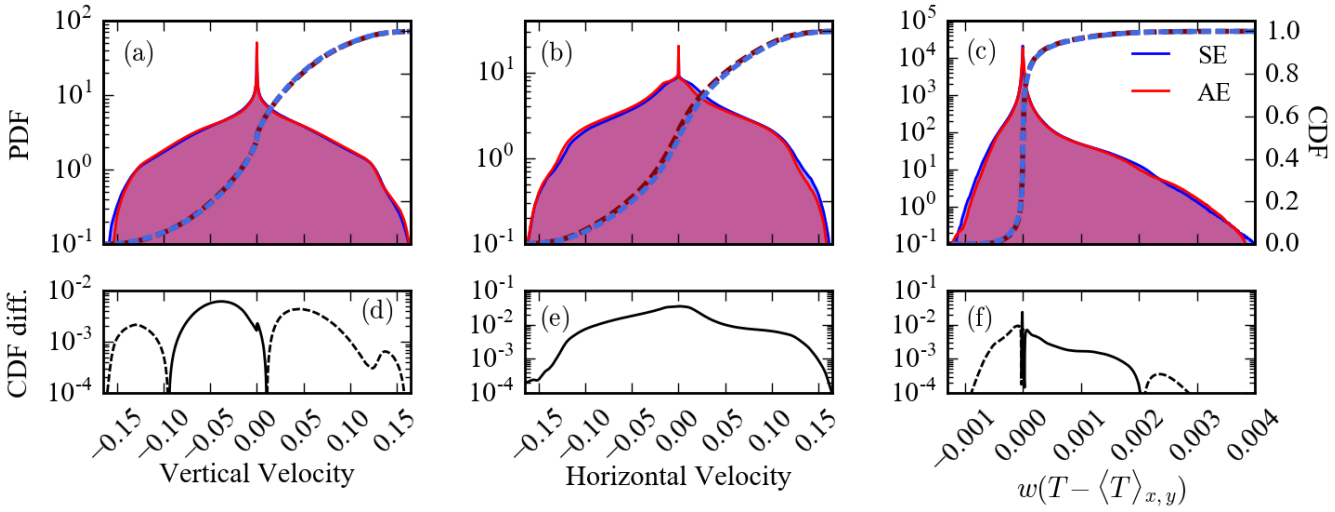

FIG. 4. Probability distribution functions of (a) the vertical velocity, (b) the horizontal velocity, and (c) nonlinear convective transport are shown for a 2D runs achieved through the SE and AE methods at $S = 10^5$. Flows are sampled every 0.1 time units for 500 total time units, and flows are interpolated onto an evenly spaced grid before sampling. The cumulative distribution function is overplotted on each plot.

4a), horizontal velocity (Fig. 4b), and the nonlinear convective flux (Fig. 4c). We report KS statistics of 0.00615, 0.0349, and 0.0263, respectively. Perhaps unsurpisingly, the nonlinear convective transport between the SE and AE methods are very similar, as is captured in a volume-averaged sense in the Nu measurements of Fig. 2a&d. Each distribution shows a strong peak near zero due to the velocity boundary conditions (Eqn. (7)), but the distribution of flux transport elements and velocities is nearly identical in the AE and SE solutions.

The small differences between the SE and AE solutions for the case studied in Figs. 1, 3, & 4, show that the AE method is extremely powerful. The first application of the AE method ($t \approx 70$ in Fig. 1b) immediately increases the average time step of our solver by a factor of 2-3. At higher supercriticality ($S = 10^7$), the AE solve immediately boosts the timestep by nearly a factor of 4. Thus, not only does this method evolve the solution into nearly the correct state, but further time evolution (either to achieve precisely the correct thermodynamic state or to take measurements of fluid quantities) happens more efficiently.

IV. EXTENSIONS & CONCLUSION

In this work we have used Rayleigh-Bénard convection as a test case for the AE method, but we argue that the true power of this technique is in its extensions to more complicated studies. One need only derive the steady-state, horizontally-averaged equations for a given equation set (e.g., Eqns. (9) & (10)) and couple that information with knowledge of the boundary conditions and current dynamics (as described in section II A and appendix A) to achieve a quickly converged solution. While in-depth studies of AE extensions are beyond the scope of this paper, we will briefly describe areas in which the AE method should be explored.

In conclusion, here we have described a procedure for converging convective simulations using a method of Accelerated Evolution (AE), and compared it to Standard Evolution (SE) achieved by running simulations for a thermal timescale. We have shown that the AE method produces evolved solutions on short timescales whose dynamics are similar to SE solutions, and we have discussed differences that arise between the two methods.

We have shown that the AE method is valid at low values of S, in which solutions converge quickly and the thermal timescale is short, but that it is also applicable at high values of S, where SE solutions can take an intractable amount of time. This shows that the AE method not only progresses solutions towards the correct evolved state (at high S), but that it also does not remove the simulation from the correct evolved state once such a state is achieved (at low S). We have studied the AE method in both 2D and 3D, but have restricted most of our study to 2D flows. Because the AE technique depends only on horizontally integrated information, we examine a select small group of 3D simulations only to demonstrate the method's efficacy there.

One area in which the AE approach can be applied is to simple studies of internally heated convection [25]. The least complex of these studies examine the incompressible Boussinesq equations, as presented in this work, but include

a constant source term in the energy equation. The evolved convective state in such internally heated systems includes a flux profile whose value linearly increases with height, as the volumetric heating requires the convection to carry more flux towards the top of the domain. These systems can be straightforwardly studied using the methods that we examined here, while scaling the profiles derived in Eqn. (8) by the proper, height-dependent flux.

Studies of stratified convection are likely to gain the most through developing and employing the AE method. In many studies of stratified convection, the thermal diffusivity is inversely proportional to the density [7]. Thus, the thermal timescale is much larger deep in the atmosphere, where density is high and diffusivity is very low, than it is near the surface. As such, runs at similar supercriticalities but with different degrees of stratification can have thermal timescales which differ by orders of magnitude. Fortunately, the AE method is easily adapted to the simplest stratified, compressible systems. Rather than studying the total flux through the domain, it is essential to study only the flux in excess of what is conducted along the adiabatic temperature gradient while constructing the profiles in Eqn. (8). Furthermore, in addition to solving for hydrostatic balance and thermal equilibrium, as in Eqns. (9) & (10), it is essential to simultaneously ensure that mass is conserved. Thus, additional equations and boundary conditions must be used to ensure that mass is not created or destroyed, in a manner similar to how mass is treated in stellar structure codes [26].

Studies of convection frequently examine paired stable and convecting regions [13, 14, 16]. When the interface between the stable region and the convecting region is stiff and motions do not cross that interface, convective motions cannot accelerate the restratification of the stable region. In fully-convective domains, such as those studied in this work, the thermodynamics evolve at a more rapid rate than the thermal diffusion time across the domain due to the help of convective motions. For example, in Fig. 1a, the SE solution is fully converged after $4 \cdot 10^3$ freefall time units, despite the thermal timescale being roughly 10^4 freefall units.

Stellar structure + 3-2-1 D [27, 28].

ACKNOWLEDGMENTS

EHA acknowledges the support of the University of Colorado's George Ellery Hale Graduate Student Fellowship. This work was additionally supported by NASA LWS grant number NNX16AC92G. Computations were conducted with support by the NASA High End Computing (HEC) Program through the NASA Advanced Supercomputing (NAS) Division at Ames Research Center on Pleiades with allocations GID s1647 and GID g26133.

Appendix A: Accelerated Evolution Recipe

In order to achieve Accelerated Evolution (AE), we pause the Direct Numerical Simulation (DNS) which is evolving the dynamics of the convection and solve a 1D Boundary Value Problem (BVP) consisting of Eqns. (9) & (10). After solving this BVP, we adjust the fields being evolved in the DNS appropriately towards their evolved state, and then we continue running the now-evolved DNS. There specific steps taken in completing the AE method are as follows:

1. After the start of the DNS, we wait some time, $t_{\text{transient}}$ after the convective transient in which the dynamics vigorously break away from the hydrostatic state.

2. Then, during the DNS, we calculate time averages of the 1D profiles of F_{conv}, F_{tot}, and $\langle \boldsymbol{u} \times \boldsymbol{\omega} \rangle_{x,y}$, updating them every timestep. To calculate these averages, we use a trapezoidal-rule integration in time, and then divide by the total time elapsed over which the average is taken.

3. We pause the DNS once the averages are sufficiently converged. To ensure that an average is converged, at least some time t_{min} must have passed since the average was started to ensure that the full range of convective dynamics are probed, and the profiles must change by no more than $P\%$ on a given timestep.

4. Construct $\text{F}_{\text{conv, ev}}$ and ξ as specified in section II A from the averaged profiles.

5. Solve the BVP for $\langle T_1 \rangle_{x,y}$ and $\langle \varpi \rangle_{x,y}$ of the evolved state. Set the horizontal average of the current DNS thermodynamic fields equal to the results of the BVP.

6. Multiply the velocity field and the temperature fluctuations, $T - \langle T \rangle_{x,y}$, by $\sqrt{\xi}$ in the DNS to properly reduce the convective flux.

7. Continue running the DNS

TABLE I. Simulation parameters

S	Ra	nz	nx, ny	$t_{\rm therm}$	$t_{\rm avg}$	$\mathrm{Nu_{SE}}$	$\mathrm{Nu_{AE}}$
$10^{1/3}$	$2.79 \cdot 10^3$	32	64	52.8	100	1.46	1.46
$10^{2/3}$	$6.01 \cdot 10^3$	32	64	77.6	100	1.95	1.95
10^{1}	$1.30 \cdot 10^4$	32	64	114	100	2.43	2.42
$10^{1+1/3}$	$2.79 \cdot 10^4$	32	64	167	100	2.54	2.54
$10^{1+2/3}$	$6.01 \cdot 10^4$	32	64	245	100	3.14	3.14
10^{2}	$1.30 \cdot 10^5$	64	128	360	100	3.8	3.8
$10^{2+1/3}$	$2.79 \cdot 10^5$	64	128	528	100	4.71	4.71
$10^{2+2/3}$	$6.01 \cdot 10^5$	64	128	776	100	5.5	5.5
10^{3}	$1.30 \cdot 10^6$	128	256	$1.14 \cdot 10^3$	200	6.4	6.33
$10^{3+1/3}$	$2.79 \cdot 10^6$	128	256	$1.67 \cdot 10^3$	500	6.87	6.95
$10^{3+2/3}$	$6.01 \cdot 10^6$	256	512	$2.45 \cdot 10^3$	500	7.54	7.59
10^{4}	$1.30 \cdot 10^7$	256	512	$3.60 \cdot 10^3$	500	8.83	8.83
$10^{4+1/3}$	$2.79 \cdot 10^7$	256	512	$5.28 \cdot 10^3$	500	10.13	10.14
$10^{4+2/3}$	$6.01 \cdot 10^7$	256	512	$7.76 \cdot 10^3$	500	11.65	11.69
10^{5}	$1.30 \cdot 10^8$	512	1024	$1.14 \cdot 10^4$	500	14.02	14.18
$10^{5+1/3}$	$2.79 \cdot 10^8$	512	1024	$1.67 \cdot 10^4$	500	–	16.21
$10^{5+2/3}$	$6.01 \cdot 10^8$	512	1024	$2.45 \cdot 10^4$	500	–	18.58
10^{6}	$1.30 \cdot 10^9$	1024	2048	$3.60 \cdot 10^4$	500	–	22.13
10^{7}	$1.30 \cdot 10^{10}$	2048	4096	$1.14 \cdot 10^5$	200	–	40.78
10^{1}	$1.30 \cdot 10^4$	32	64×64	114	100	2.42	2.42
10^{2}	$1.30 \cdot 10^5$	64	128×128	360	100	3.97	4
10^{3}	$1.30 \cdot 10^6$	128	256×256	$1.14 \cdot 10^3$	500	6.27	6.27
10^{4}	$1.30 \cdot 10^7$	256	512×512	$3.60 \cdot 10^3$	500	9.92	9.88

We refer to this process as an "AE BVP solve."

While the use of a single AE BVP solve rapidly advances the convecting state to one that is closer to the evolved state, we find that repeating this method multiple times is the best way to ensure that the AE solution is truly converged. For all runs in 2D at $S < 10^5$, we set $t_{\rm transient} = 50$, completed an AE BVP solve with $t_{\rm min} = 30$ and $P = 0.1$, and then repeated the procedure, including another wait of $t_{\rm transient} = 50$ before beginning averages. For all 3D runs and 2D runs with $S \in [10^5, 10^6]$, we did a first AE BVP solve with $t_{\rm transient} = 20$, $t_{\rm min} = 20$, and $P = 1$ in order to quickly reach a near- converged state and vastly increase our timestep size. After this first solve, we completed two AE BVP solves, with $t_{\rm transient} = 30$, $t_{\rm min} = 30$, and $P = 0.1$ to get very close to the solution (as in Fig. 1c). At very high $S = 10^7$, we ran two AE BVP solves with $t_{\rm min} = 20$ and $P = 1$. For the first solve, we set $t_{\rm transient} = 20$, and for the second we set $t_{\rm transient} = 30$. We used fewer solves at this high value of S in part to reduce the computational expense of the run, and in part because of how a third BVP generally did not modify the solution hugely (as in Fig. 1c).

Appendix B: Table of Runs

In Table I we list key properties of all simulations conducted in this work. The supercriticality, Rayleigh number, and resolution are reported. We report the simulation run time of the SE solutions and AE solutions, as well as the amount of time over which average measurements were taken, in freefall time units. The volume-averaged Nusselt number of the AE and SE solutions are shown. In the upper part of the table, information pertaining to 2D runs is reported, and below the double horizontal bars we report properties of all 3D runs.

[1] B. P. Brown, M. K. Browning, A. S. Brun, M. S. Miesch, and J. Toomre, "Persistent Magnetic Wreaths in a Rapidly Rotating Sun," Astrophys. J. **711**, 424–438 (2010), arXiv:1011.2831 [astro-ph.SR].

[2] N. A. Featherstone and B. W. Hindman, "The Spectral Amplitude of Stellar Convection and Its Scaling in the High-Rayleigh-number Regime," Astrophys. J. **818**, 32 (2016), arXiv:1511.02396 [astro-ph.SR].

[3] M. Viallet, I. Baraffe, and R. Walder, "Towards a new generation of multi-dimensional stellar evolution models: development of an implicit hydrodynamic code," Astronomy & Astrophysics **531**, A86 (2011), arXiv:1103.1524 [astro-ph.IM].

[4] M. Viallet, I. Baraffe, and R. Walder, "Comparison of different nonlinear solvers for 2D time-implicit stellar hydrodynamics," Astronomy & Astrophysics **555**, A81 (2013), arXiv:1305.6581 [astro-ph.SR].

[5] M. Viallet, T. Goffrey, I. Baraffe, D. Folini, C. Geroux, M. V. Popov, J. Pratt, and R. Walder, "A Jacobian-free Newton-Krylov method for time-implicit multidimensional hydrodynamics. Physics-based preconditioning for sound waves and thermal diffusion," Astronomy & Astrophysics **586**, A153 (2016), arXiv:1512.03662 [astro-ph.IM].

[6] D. Lecoanet, B. P. Brown, E. G. Zweibel, K. J. Burns, J. S. Oishi, and G. M. Vasil, "Conduction in Low Mach Number Flows. I. Linear and Weakly Nonlinear Regimes," Astrophys. J. **797**, 94 (2014), arXiv:1410.5424 [astro-ph.SR].

[7] E. H. Anders and B. P. Brown, "Convective heat transport in stratified atmospheres at low and high Mach number," Physical Review Fluids **2**, 083501 (2017), arXiv:1611.06580 [physics.flu-dyn].

[8] B. Bordwell, B. P. Brown, and J. S. Oishi, "Convective Dynamics and Disequilibrium Chemistry in the Atmospheres of Giant Planets and Brown Dwarfs," Astrophys. J. **854**, 8 (2018), arXiv:1802.03026 [astro-ph.EP].

[9] M. Stix, "On the time scale of energy transport in the sun," Solar Physics **212**, 3–6 (2003).

[10] H. Johnston and C. R. Doering, "Comparison of Turbulent Thermal Convection between Conditions of Constant Temperature and Constant Flux," Phys. Rev. Lett. **102**, 064501 (2009), arXiv:0811.0401 [physics.flu-dyn].

[11] R. Verzicco and R. Camussi, "Transitional regimes of low-Prandtl thermal convection in a cylindrical cell," Physics of Fluids **9**, 1287–1295 (1997).

[12] N. E. Hurlburt, J. Toomre, and J. M. Massaguer, "Two-dimensional compressible convection extending over multiple scale heights," Astrophys. J. **282**, 557–573 (1984).

[13] L.-A. Couston, D. Lecoanet, B. Favier, and M. Le Bars, "Dynamics of mixed convective-stably-stratified fluids," Physical Review Fluids **2**, 094804 (2017), arXiv:1709.06454 [physics.flu-dyn].

[14] A. Brandenburg, K. L. Chan, Å. Nordlund, and R. F. Stein, "Effect of the radiative background flux in convection," Astronomische Nachrichten **326**, 681–692 (2005), astro-ph/0508404.

[15] R. J. A. M. Stevens, D. Lohse, and R. Verzicco, "Prandtl and Rayleigh number dependence of heat transport in high Rayleigh number thermal convection," Journal of Fluid Mechanics **688**, 31–43 (2011), arXiv:1102.2307 [physics.flu-dyn].

[16] N. E. Hurlburt, J. Toomre, and J. M. Massaguer, "Nonlinear compressible convection penetrating into stable layers and producing internal gravity waves," Astrophys. J. **311**, 563–577 (1986).

[17] E. A. Spiegel and G. Veronis, "On the Boussinesq Approximation for a Compressible Fluid." Astrophys. J. **131**, 442 (1960).

[18] F. Cattaneo, N. H. Brummell, J. Toomre, A. Malagoli, and N. E. Hurlburt, "Turbulent compressible convection," Astrophys. J. **370**, 282–294 (1991).

[19] L. Korre, N. Brummell, and P. Garaud, "Weakly non-Boussinesq convection in a gaseous spherical shell," Phys. Rev. E **96**, 033104 (2017), arXiv:1704.00817 [physics.flu-dyn].

[20] K. Burns, G. Vasil, J. Oishi, D. Lecoanet, and B. Brown, "Dedalus: Flexible framework for spectrally solving differential equations," Astrophysics Source Code Library (2016), ascl:1603.015.

[21] U. M. Ascher, S. J. Ruuth, and R. J. Spiteri, "Implicit-explicit Runge-Kutta methods for time-dependent partial differential equations," Applied Numerical Mathematics **25**, 151–167 (1997).

[22] David Goluskin, Hans Johnston, Glenn R. Flierl, and Edward A. Spiegel, "Convectively driven shear and decreased heatflux," J. Fluid Mech. **759**, 360–385 (2014).

[23] J. Otero, R. W. Wittenberg, R. A. Worthing, and C. R. Doering, "Bounds on Rayleigh Bénard convection with an imposed heat flux," J. Fluid Mech. **473**, 191–199 (2002).

[24] J. V. Wall and C. R. Jenkins, *Practical Statistics for Astronomers, by J. V. Wall , C. R. Jenkins, Cambridge, UK: Cambridge University Press, 2012* (2012).

[25] David Goluskin, *Internally Heated Convection and Rayleigh-Bénard Convection* (Springer International Publishing, 2016).

[26] B. Paxton, L. Bildsten, A. Dotter, F. Herwig, P. Lesaffre, and F. Timmes, "Modules for Experiments in Stellar Astrophysics (MESA)," The Astrophysical Journal Supplement Series **192**, 3 (2011), arXiv:1009.1622 [astro-ph.SR].

[27] W. D. Arnett, C. Meakin, M. Viallet, S. W. Campbell, J. C. Lattanzio, and M. Mocák, "Beyond Mixing-length Theory: A Step Toward 321D," Astrophys. J. **809**, 30 (2015), arXiv:1503.00342 [astro-ph.SR].

[28] A. Cristini, C. Meakin, R. Hirschi, D. Arnett, C. Georgy, and M. Viallet, "Linking 1D evolutionary to 3D hydrodynamical simulations of massive stars," Physica Scripta **91**, 034006 (2016), arXiv:1601.01572 [astro-ph.SR].